

See discussions, stats, and author profiles for this publication at: <https://www.researchgate.net/publication/231646984>

Effects of Pt Particle Size on Hydrogen Storage on Pt-Doped Metal–Organic Framework IRMOF-8

ARTICLE in THE JOURNAL OF PHYSICAL CHEMISTRY C · FEBRUARY 2011

Impact Factor: 4.77 · DOI: 10.1021/jp111800c

CITATIONS

47

READS

52

4 AUTHORS, INCLUDING:



Hao Chen

Texas A&M University

18 PUBLICATIONS 125 CITATIONS

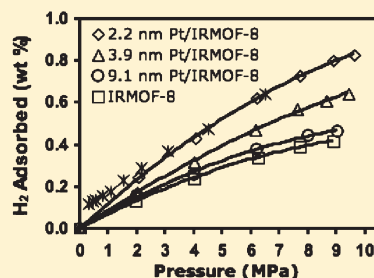
SEE PROFILE

Effects of Pt Particle Size on Hydrogen Storage on Pt-Doped Metal–Organic Framework IRMOF-8

Lifeng Wang, Nicholas R. Stuckert, Hao Chen, and Ralph T. Yang*

Department of Chemical Engineering, University of Michigan, Ann Arbor, Michigan 48109-2136, United States

ABSTRACT: A series of Pt-doped IRMOF-8 samples with different Pt catalyst sizes have been prepared via organometallic chemical-vapor deposition (CVD). The Pt catalyst size effects on the spillover storage on IRMOF-8 (or any MOF) were studied for the first time. Our studies showed that the Pt catalyst size is a crucial factor determining whether a significant enhancement in storage can be achieved in the hydrogen spillover system at ambient temperature. Compared to undoped IRMOF-8, the spillover storage capacities on Pt-doped IRMOF-8 samples were enhanced by factors ranging from 1.1 to 1.9 because of different Pt catalyst sizes. The doped Pt size was controlled by varying the CVD conditions to yield mean sizes of 2.2, 3.9, and 9.1 nm, and the results showed that smaller sizes were needed for spillover. Temperature-programmed desorption of dosed H₂/D₂ further shed light on the mechanism of spillover and reverse spillover, confirming undercoordinated sites on the particle-enhanced spillover.



1. INTRODUCTION

Hydrogen storage is one of the key issues for the realization of fuel-cell powered vehicles using hydrogen as the energy carrier.¹ Among candidate hydrogen storage adsorbents, metal–organic frameworks (MOFs), a class of porous materials constructed by coordinate bonds between multidentate ligands and metal atoms or small metal-containing clusters, have attracted increasing attention due to their lightweight, high surface area and porosity, and adjustable structures.^{2–7} Significant storages at 77 K on MOFs with high surface areas have been reported. For example, MOF-177 with a Langmuir surface area of 5640 m²/g could store the highest 7.5 wt % H₂ at 77 K and 7 MPa.^{8,9} The storage capacities of fully activated MIL-101 (Langmuir surface area 5900 m²/g) at 77 K were 3.75 wt % at 2 MPa and 6.1 wt % at 8 MPa.^{10,11} However, these significant storage capacities were achieved only at 77 K. At near ambient temperatures, the storage capacities dropped precipitously. This can be understood because hydrogen adsorption on MOFs is mostly due to weak van der Waals interactions.

To improve the hydrogen storage on adsorbents at room temperature, a most effective approach is by using hydrogen dissociation on an added catalyst followed by spillover. To date, more than 100 papers published by ~40 groups worldwide have reported significant enhancements in hydrogen storage by spillover at ambient temperatures demonstrating this technique (summarized in ref 12). Hydrogen spillover can be defined as the dissociative chemisorption of hydrogen on metal nanoparticles, and subsequent migration of hydrogen atoms onto adjacent surfaces of a receptor via surface diffusion.^{13–18} Evidence of atomic hydrogen spillover was first observed in studies of ethylene hydrogenation¹⁹ and later observed in the reduction of transition metal oxides with Pt catalyst and hydrogen uptake on transition metals supported on carbon by Khoobiar and Boudart.^{13,20,21} Direct evidence of spillover of atomic hydrogen,

at room temperature, from Pt to carbon,^{22–24} from Pt to glass,²⁵ and from Au to TiO₂²⁶ has been reported recently. The most important direct evidence for hydrogen spillover at room temperature was obtained by Mitchell et al.^{22,23} in their study of commercial Pt/C, Ru/C, and PtRu/C fuel-cell catalysts dosed with hydrogen, by using inelastic neutron scattering (INS). Their work showed a large continuum in the INS vibration spectra (at >1000 cm⁻¹) that was directly attributed to a layer of mobile H atoms on the carbon support, with a weak binding energy of 15 kJ/mol. Evidence of spillover effects on Pt-doped activated carbon by using INS was also reported by Tsao et al.²⁴ Meanwhile, theoretical studies have illustrated the facile pathway for spillover from a Pt particle onto a graphene basal plane occurs via physisorption of H atoms^{22,27,28} and thermodynamically spillover can occur from both the free-standing metal clusters and from the receptor-supported metal clusters.^{29,30} DFT studies also showed the facilitated hydrogen spillover on oxygen-modified carbons and enhanced interactions between hydrogen atom and boron-modified carbons.^{31,32} The spillover storage capacities for different MOFs and COF-1 have been calculated by Ganz and co-workers.³³ Among all transition and noble metals, the most difficult one for doping on carbon with high dispersion is Pt; recent results have shown that high dispersion (i.e., in particle sizes less than ~4 nm) is necessary for hydrogen spillover to occur (e.g., refs 34–37). Missteps in catalyst preparation and activation (prior to storage measurement) lead directly to diminished or no spillover. Common missteps and pitfalls have been pointed out recently.³⁴

Hydrogen spillover on MOFs can be facilitated by building carbon bridges between the dissociation source (e.g., commercial

Received: December 12, 2010

Revised: February 2, 2011

Published: March 01, 2011

Pt/AC catalyst) and MOFs,^{38–43} encapsulation,⁴⁴ or direct doping of dissociation metals (Pt, Pd, Ni) on MOFs.^{45–48} The thermal-desorption mass spectrometry studies by the Miller group have revealed multiple hydrogen binding sites occurring on catalyst bridged MOFs between 263 and 298 K, substantially higher than that for simple physisorbed dihydrogen.⁴¹ The factors that affect hydrogen spillover on MOFs by bridge building have been discussed.³⁴ It was suggested that the ideal situation for hydrogen spillover on bridged MOFs was when all individual catalyst and MOF receptor particles were “bridged,” which was highly empirical and difficult to achieve. Studies on direct doping of metals on MOFs for hydrogen spillover started to appear recently. Enhanced hydrogen spillover at room temperature has been observed on Pt-doped MOF-177, Ni-doped MIL-101, Pd-doped redox-active MOF, and Pd-doped MIL-100.^{45–48} Unlike the MOF-bridging technique, direct metal doping has the potential of being more controllable and hence the results more reproducible. It is known that direct doping could result in the dispersion of metal particles on MOFs, and physical and energy barriers for transfer of hydrogen atoms from one material to another exist during spillover. Thus, the dispersion and the particle size of the metal on MOFs will affect spillover and thereby the hydrogen storage on MOFs. To our knowledge, studies of catalyst dispersion and particle size effects on hydrogen storage on MOFs have not been reported. In this work, we synthesized a series of direct Pt-doped IRMOF-8 samples via organometallic chemical vapor deposition and studied the Pt dispersion and particle size effects on the hydrogen storage.

2. EXPERIMENTAL METHODS

2.1. Syntheses. *2.1.1. Synthesis of IRMOF-8.* Typically, 1.19 g of $Zn(NO_3)_2 \cdot 6H_2O$ (freshly opened) and 0.43 g of 2,6-naphthalenedicarboxylic acid were dissolved in 40 mL of diethylformamide (DEF) during vigorous stirring at room temperature.^{49,50} The DEF solution was heated to 393 K for 20 h and then cooled to room temperature. The white product was collected by filtering and four thorough washings with DMF. The product was exchanged by $CHCl_3$ four times and then degassed at 423 K for 12 h.

2.1.2. Synthesis of Pt-Doped IRMOF-8 via Chemical Vapor Deposition (CVD). Pt was doped on IRMOF-8 by chemical vapor deposition of a volatile platinum precursor (trimethyl-methylcyclopentadienyl platinum(IV)). The MOF crystals were ground before CVD. The grounded MOFs (0.6 g) and the organometallic precursor (0.09 g) were placed in a tube separated by a glass frit and degassed to a vacuum of $<10\text{ }\mu\text{mHg}$ at 273 K. After that, the degassing was stopped and the temperature was increased to 303 K and maintained at 303 K for 1 h. The vacuum of this system was renewed each hour for six cycles and then stayed for another 6 h. During this procedure, an off-white composite was yielded and designated as Pt/IRMOF-8-1. For Pt/IRMOF-8-2 sample, the temperature was kept at 308 K and the vacuum was renewed each hour for four cycles and then stayed for another 8 h. For Pt/IRMOF-8-3 sample, the temperature was maintained at 318 K and the vacuum was renewed for one cycle and then stayed 11 h. These three samples were reduced in a hydrogen atmosphere at 423 K overnight and then purged with flowing helium. Finally, the Pt/IRMOF-8-1 with 4.8 wt % Pt, Pt/IRMOF-8-2 with 6.2 wt % Pt, and Pt/IRMOF-8-3 with 7.7 wt % Pt were obtained.

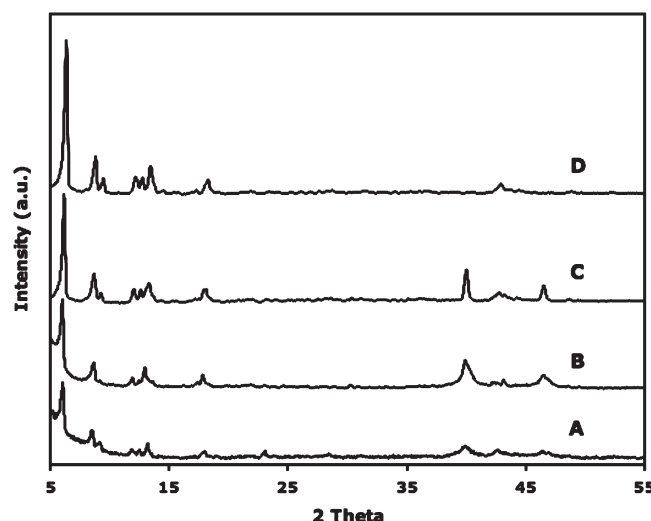


Figure 1. XRD patterns of Pt/IRMOF-8-1 (A), Pt/IRMOF-8-2 (B), Pt/IRMOF-8-3 (C), and pure IRMOF-8 (D).

2.2. Sample Characterization and Isotherm Measurements. Powder X-ray diffraction (XRD) data were recorded on a Rigaku Miniflex diffractometer at 30 kV, 15 mA for $Cu K\alpha$ ($\lambda = 0.1543\text{ nm}$) radiation, with a step size of 0.02° in 2θ . Transmission electron microscopy (TEM) images were obtained on a JEOL 3011 analytical electron microscope equipped with EDX analysis operated at 300 kV. Nitrogen adsorption and low-pressure H_2 adsorption isotherms ($0\text{--}1\text{ atm}$) were measured with a standard static volumetric technique (Micromeritics ASAP 2020). Hydrogen adsorption at 298 K and pressures greater than 0.1 MPa and up to 10 MPa was measured using a static volumetric technique with a specially designed Sieverts-type apparatus. The apparatus was previously tested and proven to be leak-free and accurate through calibration by using $LaNi_5$, AX-21, Maxsorb, zeolites, and MOFs at 298 K.⁵¹ The best standard calibration material for high-pressure hydrogen storage measurement is the commercial superactivated carbon, AX-21 or Maxsorb. The storage capacity for AX-21 (BET S.A. = $2800\text{ m}^2/\text{g}$) at 10 MPa and 298 K should be 0.6 wt % while that for Maxsorb (BET S.A. = $3300\text{ m}^2/\text{g}$) should be 0.7 wt % under the same conditions, both with a slightly concave-shaped isotherm. Approximately 200 mg of sample was used for each high-pressure isotherm measurement in this study.

Temperature-programmed desorption (TPD) was used to identify high-energy binding. A 100 mg sample was dosed with hydrogen for a period of time and cooled to 77 K under pressure. Excess gas was vacuumed off and the sample was heated at a constant rate while the evolved gas was monitored with a mass spectrometer (MS).

3. RESULTS AND DISCUSSION

Powder X-ray diffraction patterns of IRMOF-8 and Pt/IRMOF-8 samples are shown in Figure 1. The plain IRMOF-8 (Figure 1D) showed typical peaks at $2\theta = 6.3^\circ$, in good agreement with previous reports.^{49,50} After IRMOF-8 was doped with Pt, the XRD patterns of Pt/IRMOF-8-1, Pt/IRMOF-8-2, and Pt/IRMOF-8-3 samples all exhibited the same peaks as those of plain IRMOF-8, although the peak intensity decreased slightly. This indicates that the microstructure of IRMOF-8 was retained after the doping treatments. Furthermore, the Pt/IRMOF-8

samples all showed two peaks at ca. 40° and 46° , characteristic of the metallic platinum particles. These results confirm that Pt metals were successfully doped on IRMOF-8 by applying the CVD method. It is noted that the peaks corresponding to Pt became narrower from Pt/IRMOF-8-1 to Pt/IRMOF-8-2 and Pt/IRMOF-8-3. This indicates that the Pt particle size increased in the order of Pt/IRMOF-8-1 < Pt/IRMOF-8-2 < Pt/IRMOF-8-3.

Nitrogen adsorption was further employed to evaluate the porosity of plain IRMOF-8 and the doped samples. As shown in Figure 2, the isotherms of IRMOF-8 and Pt/IRMOF-8 samples all exhibited the type I curve, thus revealing the presence of microporosity in the samples. The BET surface area and pore volume of the plain IRMOF-8 are $1430 \text{ m}^2/\text{g}$ and $0.69 \text{ cm}^3/\text{g}$, respectively. These textural properties are in agreement with previous reports.^{49,50} After Pt was doped on IRMOF-8, the BET surface areas and pore volumes of Pt/IRMOF-8-1, Pt/IRMOF-8-2, and Pt/IRMOF-8-3 samples were reduced to 1175, 1071, and $1014 \text{ m}^2/\text{g}$ and 0.59, 0.53, and $0.55 \text{ cm}^3/\text{g}$, respectively (Table 1). The BET surface area and pore volume of Pt/IRMOF-8-1, Pt/IRMOF-8-2, and Pt/IRMOF-8-3 were lower than that of the plain IRMOF-8. This is due to the increased weight and partial micropore blockage caused by the doped Pt particles.

High-pressure hydrogen isotherms at 298 K for the plain IRMOF-8, Pt/IRMOF-8-1, Pt/IRMOF-8-2, and Pt/IRMOF-8-3 samples are presented in Figure 3. As shown in Figure 3, IRMOF-8 had a hydrogen storage capacity of $\sim 0.44 \text{ wt } \%$ at 298 K and 10 MPa. After Pt was doped on IRMOF-8, the hydrogen uptakes on Pt/IRMOF-8-1, Pt/IRMOF-8-2, and Pt/IRMOF-8-3 at 10 MPa were enhanced to 0.85, 0.67, and 0.49 wt %, respectively (Table 1). It can be seen that all the Pt/IRMOF-8 samples exhibited higher hydrogen adsorption capacity than the plain

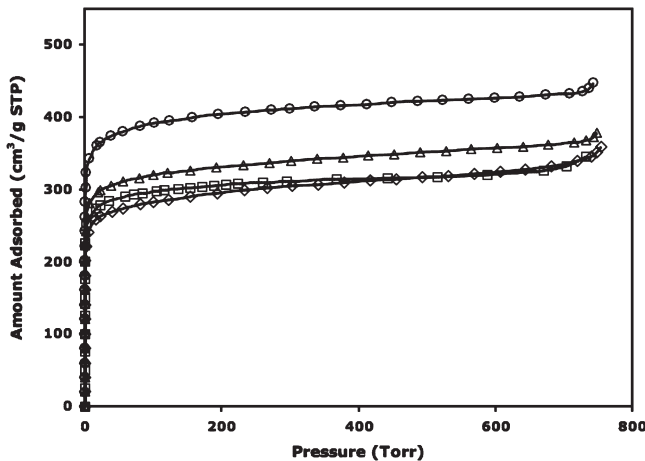


Figure 2. Nitrogen isotherms of Pt/IRMOF-8-1 (Δ), Pt/IRMOF-8-2 (\square), Pt/IRMOF-8-3 (\diamond), and pure IRMOF-8 (\circ).

IRMOF-8 sample up to 10 MPa. The enhanced hydrogen storage capacity could not be attributed to differences in surface area because the Pt/IRMOF-8 samples have lower surface area than that of the plain IRMOF-8, as shown by nitrogen adsorption results. The enhancement of hydrogen storage was attributed to the spillover of atomic hydrogen from Pt particles to IRMOF-8. The Ru, Pt, Pd, and Ni metals are known as hydrogen dissociation sources, and the enhanced hydrogen storage on various supports by doping these metals has been well observed.^{12–48} Another feature observed in the isotherms of Pt/IRMOF-8 was the near linearity. As shown in our previous work as well as in the results by other groups, the spillover isotherms usually appear to be nearly linear. The near linearity in the isotherms has been explained by our phenomenological spillover isotherm model,⁵² and indicates that the spillover amounts are far from reaching the limiting capacities.¹²

It is noted that, in our case, the hydrogen storage capacity followed the order of Pt/IRMOF-8-1 > Pt/IRMOF-8-2 > Pt/IRMOF-8-3. The maximum hydrogen uptake reached 0.85 wt % at 10 MPa on Pt/IRMOF-8-1. The reversibility on Pt/IRMOF-8-1 was also evaluated by measuring the desorption branch down to 1 atm. It can be seen that the desorption branch nearly followed the adsorption branch, although there appeared to be a slight hysteresis. After evacuation to a pressure of 1 Pa for 12 h at 298 K, total desorption occurred. The second adsorption isotherm was essentially the same as the first adsorption isotherm. The slight hysteresis between the adsorption and desorption branch is likely due to spillover hydrogen atoms adsorbed on the defective sites on IRMOF-8. The hysteresis is not obvious on Pt/IRMOF-8-3 since less spillover hydrogen adsorption occurred on it. In comparison with the pristine IRMOF-8, it is notable that the hydrogen adsorption amount of Pt/IRMOF-8-1 was enhanced

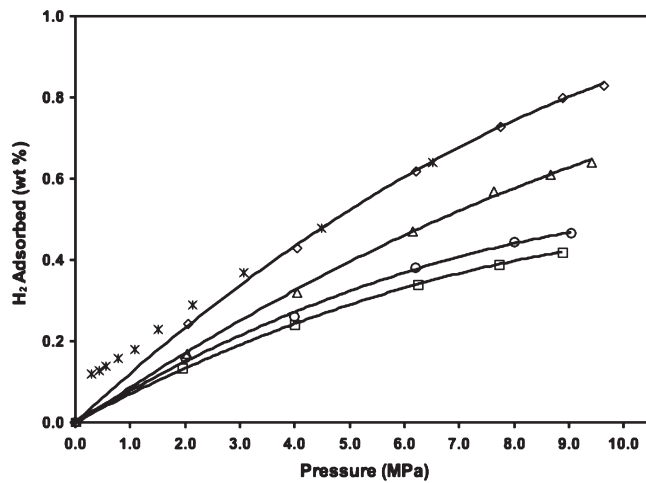


Figure 3. High-pressure hydrogen adsorption isotherms at 298 K for plain IRMOF-8 (\square), Pt/IRMOF-8-1 (\diamond), Pt/IRMOF-8-2 (\triangle), and Pt/IRMOF-8-3 (\circ) samples and desorption on Pt/IRMOF-8-1 (*).

Table 1. Textural Parameters, Pt Content, Pt Size, and Hydrogen Uptake on Various Samples

sample	BET surface area (m^2/g)	pore volume (cm^3/g)	Pt content (wt %)	average Pt size (nm)	H_2 uptake at 10 MPa (wt %)
IRMOF-8	1430	0.69			0.44
Pt/IRMOF-8-1	1175	0.59	4.8	2.2	0.85
Pt/IRMOF-8-2	1071	0.53	6.2	3.9	0.67
Pt/IRMOF-8-3	1014	0.55	7.7	9.1	0.49

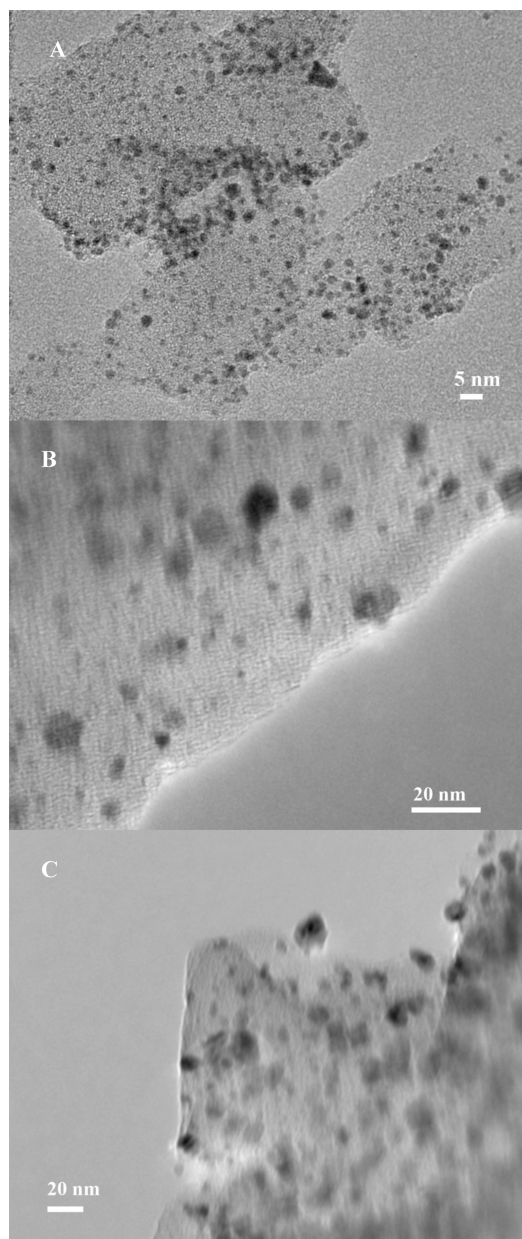


Figure 4. TEM images of Pt/IRMOF-8-1 (A), Pt/IRMOF-8-2 (B), and Pt/IRMOF-8-3 (C).

by a factor of 1.9 (or a 90% increase). However, the enhancement factors were only 1.5 for Pt/IRMOF-8-2 and 1.1 for Pt/IRMOF-8-3. It is noted that the Pt content difference in the present study (from 4.8 to 7.7 wt %) should not affect the enhancement significantly. Previous studies have shown significant enhancements when the Pt content was ~5–7 wt %.^{36,56,57}

The variation in the storage capacities of Pt/IRMOF-8 samples indicates that differences existed among the samples. The Pt/IRMOF-8 samples were characterized by TEM and chemisorption analyses. TEM images of Pt/IRMOF-8-1, Pt/IRMOF-8-2, and Pt/IRMOF-8-3 samples are shown in Figure 4. For each doped sample, the dark spots of Pt particles could be observed. These results further confirm Pt has been successfully doped on the MOF support. The Pt particle size increased with the order of Pt/IRMOF-8-1 < Pt/IRMOF-8-2 < Pt/IRMOF-8-3. The mean particle sizes with standard deviations were 2.2 ± 1.0 nm

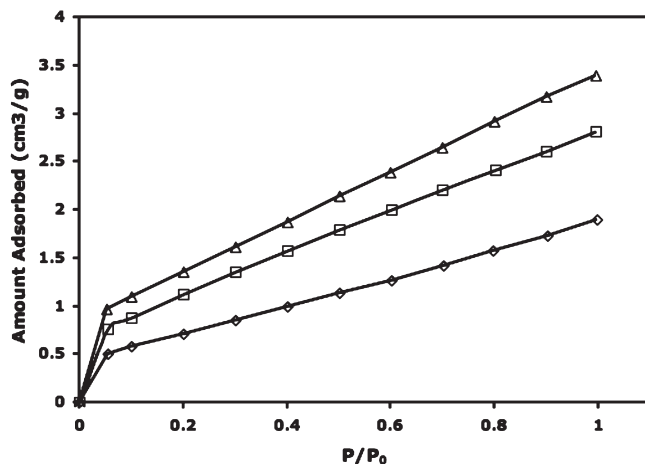


Figure 5. Hydrogen isotherms of Pt/IRMOF-8-1 (Δ), Pt/IRMOF-8-2 (\square), and Pt/IRMOF-8-3 (\diamond).

for Pt/IRMOF-8-1, 3.9 ± 1.9 nm for Pt/IRMOF-8-2, and 9.1 ± 4.3 nm for Pt/IRMOF-8-3. As TEM yielded limited information of the Pt dispersion on the whole sample, hydrogen chemisorption was further used to estimate the metal dispersion. It is known that the Benson–Boudart method is a good assessment for the dispersion of metals on supports. From the adsorbed amount of hydrogen extrapolated to zero pressure, the dispersion of Pt metal on IRMOF-8 can be calculated. Figure 5 shows the H₂ adsorption isotherms on Pt/IRMOF-8-1, Pt/IRMOF-8-2, and Pt/IRMOF-8-3 at 298 K. It is obvious that the dispersion of Pt on MOF followed the order Pt/IRMOF-8-1 > Pt/IRMOF-8-2 > Pt/IRMOF-8-3. These results indicate high dispersion and small sizes of Pt particles facilitate spillover on MOFs and in turn the storage capacity. This is in agreement with the XRD and TEM results. The catalyst size effects on spillover storage on MOF also agreed with the previous studies on carbon receptors doped with various metals. Tsao et al. impregnated activated carbon with Pt particles of ~1–2 nm and achieved an enhancement factor of 3.³⁵ Chung et al. doped Pt particles (2 nm) on boron-substituted carbon and obtained a storage capacity 5 times higher than the activated carbon with the same surface area.³⁶ A high storage capacity on multiwalled carbon nanotubes with a good Pt dispersion was reported by Park's group.³⁷ Arenillas et al. measured the hydrogen adsorption on carbon nanospheres doped with different loadings of Ni and found that the storage capacity of doped carbon was enhanced by a factor of 1.4 to 2.3.³³ The highest storage capacity was obtained on Ni-doped carbon nanospheres with the best Ni distribution and smaller Ni particles (5 nm). Tsai's group reported that uniformly distributed Ni nanoparticles (2.3 nm) tripled the hydrogen uptake on CNTs.³⁴ Sandi's group reported the hydrogen uptake on Pd-doped carbon nanofibers was 4 times larger than that on the undoped carbon and attributed the enhancement to small Pd particles.³⁵ Our recent study on templated carbon doped with various metals (Ru, Pt, and Ni) also indicated nanosized catalysts favored high storage capacity.⁵⁶ By considering the carbon nature of the linker of MOFs, it is reasonable to observe the high dispersion and small size of Pt particles facilitated the storage capacity of MOF samples. Our previous studies showed that there is a limited area of influence for each particle due to diffusion resistance and lack of diffusion pathways.⁵⁷ Thus, particles with lower and uneven dispersion cannot affect the entire MOF support, thus

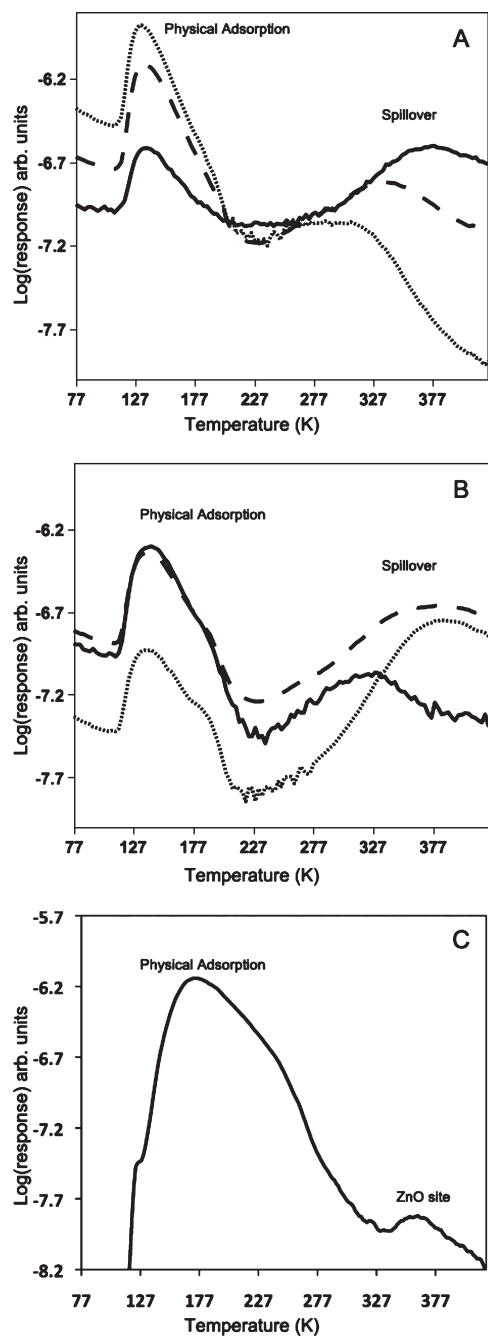


Figure 6. The TPD spectra for Pt/IRMOF-8-1. (A) H₂ was dosed for 1 h at 298 K and 300 Torr. D₂ was subsequently dosed without evacuation but left ~22 Torr of H₂ and 300 Torr D₂ for 30 min at 298 K. (B) D₂ was dosed for 24 h at 298 K and 300 Torr. H₂ was subsequently dosed without evacuation but left ~22 Torr of D₂ and 400 Torr H₂ for 15 min at 298 K. (C) For plain IRMOF-8 H₂ was dosed for 1 h at 298 K and 300 Torr. H₂ (—), D₂ (...), and HD (---).

resulting in diminished spillover enhancement. The high dispersion and small size of Pt particles contribute to increased contacts with the MOF receptor.

The size of the doped metal is affected by many factors, including the type of metal, the doping/addition rate and loading amount of the metal precursor, and the treatment temperature and metal reduction method. In our case, for doping Pt via CVD method, slower doping led to smaller particles, and the rate of

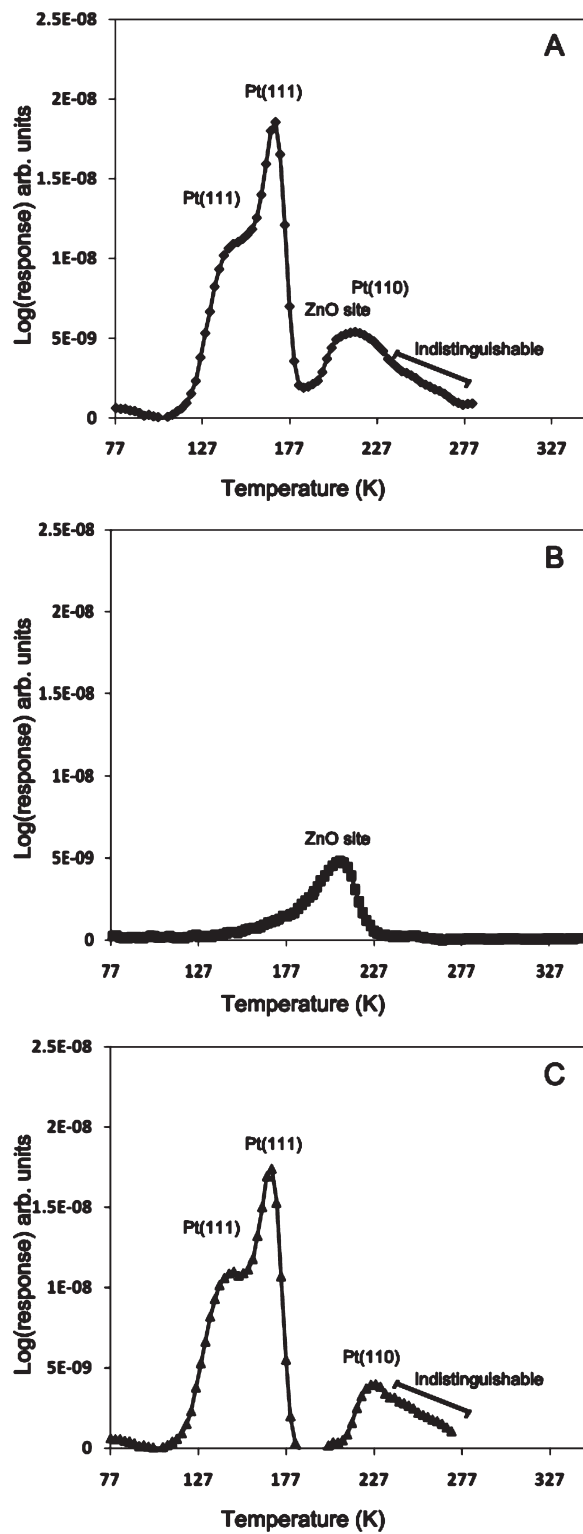


Figure 7. The TPD spectra for Pt/IRMOF-8-1 and IRMOF-8 at low pressure. D₂ was dosed for 5 min at 298 K and 25 Torr, then quenched, evacuated, and heated at a rate of 10 K/min. Spectra were cut off before observed spillover peaks to better show the other peaks. (A) Pt/IRMOF-8, (B) IRMOF-8, and (C) difference between A and B (showing only Pt contributions). The peaks are labeled corresponding to Pt binding sites derived from reference sources.^{61–64}

doping could be controlled by a number of factors. Thus, a lower temperature provided a lower Pt precursor vapor concentration,

aided by more evacuation/doping cycles, and were favorable for the uniform interactions between precursor and MOFs and, consequently, smaller particles with more even distribution. The highest doping temperature and only one evacuation/doping cycle resulted in the largest Pt size. This is similar to the effects of addition rate and concentration of H_2PtCl_6 on Pt dispersion on AX-21.³⁴ However, further optimizing the doping conditions is still needed for more significant storage enhancements.

To provide evidence for reverse spillover on Pt/IRMOF-8, sequential H_2/D_2 dosing followed by TPD experiments were carried out. The TPD spectra detailed in Figure 6 show the spillover of hydrogen as previously observed on other metal-doped supports,^{58,59} and additionally on our other work on templated carbon,⁵⁷ activated carbon,³⁴ and graphene (which does not need a metal dissociation source).⁶⁰ In this figure, we showed that if hydrogen was dosed first followed by dosing deuterium, then deuterium was desorbed first followed by hydrogen, i.e., in a reversed sequence. We also took the time to reverse the procedure and showed that this was independent of the isotopes. The peaks are labeled for simplicity to show the observed spillover peak when platinum was present, and the sole physical adsorption peaks with plain IRMOF-8 (the peak above room temperature at 350 K most likely is an internal binding site from the ZnO center, as it does not show any other signs of spillover).

One of the surprising features of the spectra in Figure 6 was the presence of a physically adsorbed peak at 135 K (present on plain IRMOF-8 as shown in Figure 6C, which seemed to have a knee at 181 K, for both IRMOF-8 and doped IRMOF-8. We examined this further in Figure 7, where we lowered the dosing pressure to 25 Torr and exposed only deuterium for 5 min (the figure shows both Pt-doped IRMOF-8, plain IRMOF-8, and the difference between the two) and then cut off before the observed spillover peaks. It is worth noting that Figure 6 was measured with long dosing times to allow enough spillover to be detected while Figure 7 was measured with short dosing times to mainly detect the hydrogen that was adsorbed on Pt. This illuminated three separate peaks for the Pt-doped IRMOF-8, not present on plain IRMOF-8. The three peaks at 135, 168, and 225 K shown in Figure 7C were all saturated at a very low pressure, indicating strong chemisorption. This is normally found on binding sites for platinum.⁶¹ The tail on the 225 K peak is of interest to identify more binding sites on the platinum, but could not be resolved with the instrument due to very low concentrations of those sites.

We then compared these platinum peaks across single-crystal spectra for platinum from the literature data. TPD spectra from the Pt(111),⁶¹ (100),⁶² and (110)⁶³ faces showed that the most likely configuration was the (111) and (110) faces. Information gained from spectra of the (210) and (211) faces⁶⁴ showed that while these were not responsible for the observed peaks, steps and edges would create very different binding sites that might contribute to the other partially obscured peaks. From the TEM observations, we could see that the particles (which were ~ 2 nm) had the characteristics observed in our earlier publication³⁴ of containing both (111) and (110) faces. Here, however, the lattice constant of IRMOF-8 does not match with the (111) surface, leaving it exposed. Building off our previous results, we could start to see that unsaturated platinum surfaces (edges, corners, defects, etc.) were present in successful spillover adsorbents.³⁴ While the dispersion of the metal still influences the storage capacity based purely on more efficient metal utilization and greater area of influence, the unsaturated sites are necessary to

perform the spillover. This should align well with previous criticisms that observe the binding energy from a single hydrogen atom on planar platinum is very strong, but weaker secondary and tertiary hydrogen adsorbs on undercoordinated sites, and supporting observations that smaller platinum is necessary to see any spillover in any observable amount.¹²

4. CONCLUSIONS

In this work, a series of Pt-doped IRMOF-8 samples have been prepared via organometallic chemical vapor deposition. The catalyst (Pt) size was affected by the doping temperature and number of doping cycles. The hydrogen storage studies showed the storage capacities via hydrogen spillover on Pt-doped IRMOF-8 samples were enhanced by a factor 1.1–1.9 when compared to that of undoped IRMOF-8. Catalyst size was a crucial factor that determined the enhancements of the storage capacity of Pt-doped MOFs. The TPD results confirmed the existence of reverse spillover on the Pt-doped IRMOF-8. The comparison to other platinum surfaces from platinum isolated TPD peaks showed that smaller particles were necessary to create higher energy sites that were needed to cause spillover. This supports information originally reported by Konvalinka and Scholten on Pd/carbon.⁵⁹

■ AUTHOR INFORMATION

Corresponding Author

*Fax: (734) 764-7453. E-mail: yang@umich.edu.

■ ACKNOWLEDGMENT

This work was supported by the NSF grant CBET-0753008 and Ford University Research Program from Ford Motor Company.

■ REFERENCES

- (1) *A Multiyear Plan for the Hydrogen R&D Program*; Office of Power Delivery, Office of Power Technologies, Energy Efficiency and Renewable Energy, Department of Energy: Washington, DC, 1999.
- (2) Seayad, A. M.; Antonelli, D. M. *Adv. Mater.* **2004**, *16*, 765.
- (3) Frost, H.; Snurr, R. Q. *J. Phys. Chem. C* **2007**, *111*, 18794.
- (4) Roswell, J.; Yaghi, O. M. *Angew. Chem., Int. Ed.* **2005**, *44*, 4670.
- (5) Murray, L. J.; Dinca, M.; Long, J. R. *Chem. Soc. Rev.* **2009**, *38*, 1294.
- (6) Collins, D. J.; Zhou, H.-C. *J. Mater. Chem.* **2007**, *30*, 3154.
- (7) Zhao, D.; Yuan, D.; Zhou, H.-C. *Energy Environ. Sci.* **2008**, *1*, 222.
- (8) Chae, H.; Siberio-Perez, D. Y.; Kim, J.; Go, Y.; Eddaoudi, M.; Matzger, A.; O'Keeffe, M.; Yaghi, O. M. *Nature* **2004**, *427*, 523.
- (9) Furukawa, H.; Miller, M.; Yaghi, O. M. *J. Mater. Chem.* **2007**, *17*, 3197.
- (10) Ferey, G.; Mellot-Draznieks, C.; Serre, C.; Millange, F.; Dutour, J.; Surble, S.; Margiakaki, I. *Science* **2005**, *309*, 2040.
- (11) Latroche, M.; Surblé, S.; Serre, C.; Mellot-Draznieks, C.; Llewellyn, P. L.; Lee, J.-H.; Chang, J.-S.; Jhung, S. H.; Férey, G. *Angew. Chem., Int. Ed.* **2006**, *45*, 8227.
- (12) Wang, L.; Yang, R. T. *Catal. Rev.—Sci. Eng.* **2010**, *54*, 411.
- (13) Robell, A. J.; Ballou, E. V.; Boudart, M. *J. Phys. Chem.* **1964**, *68*, 2748.
- (14) Srinivas, S. T.; Rao, P. K. *J. Catal.* **1994**, *148*, 470.
- (15) Conner, W. C., Jr.; Falconer, J. L. *Chem. Rev.* **1995**, *95*, 759.
- (16) Pajonk, G. M. *Appl. Catal., A* **2000**, *202*, 157.
- (17) Bond, G. C. *Metal-Catalyzed Reactions of Hydrocarbons*; Twigg, M. V., Spencer, M. S., Eds.; Springer: New York, 2005; p 118.
- (18) Wang, L.; Yang, R. T. *Energy Environ. Sci.* **2008**, *1*, 268.
- (19) Sinfelt, J. H.; Lucchesi, P. J. *J. Am. Chem. Soc.* **1963**, *85*, 3365.
- (20) Khoobiar, S. *J. Phys. Chem.* **1964**, *68*, 411.

- (21) Boudart, M.; Aldag, A. W.; Vannice, M. A. *J. Catal.* **1970**, *18*, 46.
- (22) Mitchell, P. C. H.; Ramirez-Cuesta, A. J.; Parker, S. F.; Tomkinson, J.; Thompsett, D. *J. Phys. Chem. B* **2003**, *107*, 6838.
- (23) Mitchell, P. C. H.; Ramirez-Cuesta, A. J.; Parker, S. F.; Tomkinson, J. *J. Mol. Struct.* **2003**, *651–653*, 781.
- (24) Tsao, C.-S.; Liu, Y.; Li, M.; Zhang, Y.; Leao, J. B.; Chang, H.-W.; Yu, M.-S.; Chen, S.-H. *J. Phys. Chem. Lett.* **2010**, *1*, 1569.
- (25) Zhan, D.; Velmurugan, J.; Mirkin, M. V. *J. Am. Chem. Soc.* **2009**, *131*, 14756.
- (26) Panayotov, D. A.; Yates, J. T., Jr. *J. Phys. Chem. C* **2007**, *111*, 2959.
- (27) Chen, L.; Cooper, A. C.; Pez, G. P.; Cheng, H. S. *J. Phys. Chem. C* **2007**, *111*, 18995.
- (28) Sha, X.; Knippenberg, M. T.; Cooper, A. C.; Pez, G. P.; Cheng, H. S. *J. Phys. Chem. C* **2008**, *112*, 17465.
- (29) Singh, A. K.; Ribas, M. A.; Yakobson, B. I. *ACS Nano* **2009**, *3*, 1657.
- (30) Lin, Y.; Ding, F.; Yakobson, B. I. *Phys. Rev. B: Condens. Matter.* **2008**, *78*, 041402-1.
- (31) Psوفогианакис, G. M.; Froudakis, G. E. *J. Phys. Chem. C* **2009**, *113*, 14908.
- (32) Zhu, Z. H.; Lu, G. Q.; Hatori, H. *J. Phys. Chem. B* **2006**, *110*, 1249.
- (33) Suri, M.; Dornfeld, M.; Ganz, E. *J. Chem. Phys.* **2009**, *131*, 174703.
- (34) Stuckert, N. R.; Wang, L.; Yang, R. T. *Langmuir* **2010**, *26*, 11963.
- (35) Tsao, C. S.; Tzeng, Y. R.; Yu, M. S.; Wang, C. Y.; Tseng, H. H.; Chung, T. Y.; Wu, H. C.; Yamamoto, T.; Kaneko, K.; Chen, S. H. *J. Phys. Chem. Lett.* **2010**, *1*, 1060.
- (36) Jeong, Y.; Chung, T. C. M. *Carbon* **2011**, *49*, 140.
- (37) Park, S.-J.; Lee, S.-Y. *Int. J. Hydrogen Energy* **2010**, *35*, 13048.
- (38) Li, Y.; Yang, R. T. *J. Am. Chem. Soc.* **2006**, *128*, 8136.
- (39) Yang, R. T.; Li, Y. W.; Lachawiec, A. J. *2007 Annual Progress Report, DOE Hydrogen Program*; U.S. Department of Energy: Washington, DC, 2007; IV.C.1b, 539.
- (40) Wang, C.-Y.; Tsao, C.-S.; Yu, M.-S.; Liao, P.-Y.; Chung, T.-Y.; Wu, H.-C.; Miller, M. A.; Tzeng, Y.-R. *J. Alloys Compd.* **2010**, *492*, 88.
- (41) Miller, M. A.; Wang, C.-Y.; Merrill, G. N. *J. Phys. Chem. C* **2009**, *113* (8), 3222–3231.
- (42) Tsao, C.-S.; Yu, M.-S.; Wang, C.-Y.; Liao, P.-Y.; Chen, H.-L.; Jeng, U.-S.; Tzeng, Y.-R.; Chung, T.-Y.; Wu, H.-C. *J. Am. Chem. Soc.* **2009**, *131*, 1404.
- (43) Liu, Y.-Y.; Zeng, J.-L.; Zhang, J.; Xu, F.; Sun, L.-X. *Int. J. Hydrogen Energy* **2007**, *32*, 4005.
- (44) Yang, S. J.; Cho, J. H.; Nahm, K. S.; Park, C. R. *Int. J. Hydrogen Energy* **2010**, *35*, 13062.
- (45) Liu, Y. Y.; Zhang, J.; Zeng, J. L.; Chu, H. L.; Xu, F.; Sun, L. X. *Chin. J. Catal.* **2008**, *29*, 655.
- (46) Proch, S.; Herrmannsdofer, J.; Kempe, R.; Kern, C.; Jess, A.; Seyfarth, L.; Senker, J. *Chem.—Eur. J.* **2008**, *14*, 8204.
- (47) Zlotea, C.; Campesi, R.; Cuevas, F.; Leroy, E.; Dibandjo, P.; Vollkruger, C.; Loiseau, T.; Ferey, G.; Latroche, M. *J. Am. Chem. Soc.* **2010**, *132*, 2991.
- (48) Cheon, Y. E.; Suh, M. P. *Angew. Chem., Int. Ed.* **2009**, *48*, 2899.
- (49) Yaghi, O. M.; Eddaoudi, M.; Li, H.; Kim, J.; Rosi, N. U.S. Patent No. 6,930,193 B2, 2005.
- (50) Tsao, C. S.; Yu, M. S.; Chung, T. Y.; Wu, H. C.; Wang, C. Y.; Chang, K. S.; Chen, H. L. *J. Am. Chem. Soc.* **2007**, *129*, 15997.
- (51) Lachawiec, A. J.; DiRaimondo, T. R.; Yang, R. T. *Rev. Sci. Instrum.* **2008**, *79*, 063906.
- (52) Li, Y.; Yang, F. H.; Yang, R. T. *J. Phys. Chem. C* **2007**, *111*, 3405.
- (53) Zubizarreta, L.; Menndez, J. A.; Pis, J. J.; Arenillas, A. *Int. J. Hydrogen Energy* **2009**, *34*, 3070.
- (54) Lin, K.-Y.; Tsai, W.-T.; Yang, T.-J. *J. Power Sources* **2011**, *196* (7), 3389–3394 10.1016/j.jpowsour.2010.04.026.
- (55) Back, C.-K.; Sandi, G.; Prakash, J.; Hranisavljevic, J. *J. Phys. Chem. B* **2009**, *110*, 16225.
- (56) Wang, L.; Yang, R. T. *J. Phys. Chem. C* **2008**, *112*, 12486.
- (57) Lachawiec, A. J.; Yang, R. T. *Langmuir* **2008**, *24*, 6159.
- (58) Benson, J. E.; Kohn, H. W.; Boudart, M. *J. Catal.* **1966**, *5*, 307.
- (59) Konvalinka, J. A.; Scholten, J. J. F. *J. Catal.* **1977**, *48*, 374.
- (60) Wang, L.; Stuckert, N. R.; Yang, R. T. *AICHE J.* **2011** 10.1002/aic.12470.
- (61) McCabe, R. W.; Schmidt, L. D. *Surf. Sci.* **1976**, *60*, 85.
- (62) McCabe, R. W.; Schmidt, L. D. *Surf. Sci.* **1977**, *65*, 189.
- (63) Shern, C. S. *Surf. Sci.* **1992**, *264*, 171.
- (64) McCabe, R. W.; Schmidt, L. D. *Surf. Sci.* **1977**, *66*, 101.